energies

MDPI

Article

Techno-Economic and Environmental Analysis of an Optimized Hydrogen Refueling Station Integration in a Renewable Energy Microgrid †

Roberta Tatti , Mario Petrollese * and Matteo Marchionni

Department of Mechanical, Chemical and Materials Engineering, University of Cagliari, 09123 Cagliari, Italy; roberta.tatti@unica.it (R.T.); matteo.marchionni@unica.it (M.M.)

* Correspondence: mario.petrollese@unica.it

† This paper is an extended version of our conference paper presented at the 37th International Conference on Efficiency, Cost, Optimization, Simulation and Environmental Impact of Energy Systems (ECOS 2024), Rhodes, Greece, 30 June–5 July 2024.

Abstract

Fuel cell electric vehicles represent a promising option for reducing greenhouse gas emissions from heavy-duty transport. In this context, integrating Hydrogen Refueling Stations (HRSs) into renewable-based microgrids represents a key strategy for ensuring sustainable hydrogen production. This study investigates the integration of an HRS into a photovoltaic-based microgrid supplying a fleet of 21 urban buses. A detailed hourly model of the photovoltaic system, battery storage, hydrogen generator, hydrogen storage, compression and refueling processes was developed. A multi-objective optimization was performed to minimize the Levelized Cost of Hydrogen (LCOH) while maximizing the Self-Sufficiency Rate (SSR). Three Energy Management Strategies (EMSs) were compared: hydrogen production using only renewable electricity, mixed renewable and grid electricity and grid-only electricity. Results reveal a marked economic penalty associated with achieving full self-sufficiency. Under the renewable-only EMS, the LCOH increases from 16.8 €/kg at an SSR of about 80% for the minimum-LCOH solution to 24.3 €/kg at an SSR of 100%. Under the MIXED-EMS, it increases from 12.3 €/kg at an SSR of about 47% to 22.7 €/kg at an SSR of 100%. When revenues from surplus electricity export are included, the corresponding LCOH values at 100% SSR decrease to approximately 15 €/kg, regardless of the EMS adopted. Compared with the emissions from the diesel-bus fleet, hydrogen buses could reduce emissions by about 12% with grid-based production and up to 99% with renewable hydrogen.

Keywords: green hydrogen; hydrogen storage system; energy management strategy; renewable energy microgrid; optimization model; hydrogen refueling station

Check for updates

Academic Editor: Yu Guan

Received: 29 June 2026
Revised: 31 July 2026
Accepted: 2 August 2026
Published: 5 August 2026

1. Introduction

Given the continued increase in Greenhouse Gas (GHG) emissions in recent years, sustainable solutions must be explored and encouraged in order to prevent the global average temperature from rising above 1.5 °C [1].

In this context, it is necessary to identify and promote alternative solutions to reduce GHG emissions [2], particularly in the transport sector, where conventional internal combustion engine vehicles still dominate the global fleet [3].

Recently, sustainable vehicles have become increasingly widespread. Electric vehicles are typically categorized into two main types: Battery Electric Vehicles (BEVs) and Fuel Cell Electric Vehicles (FCEVs), both emission-free during operation [4–6]. According to data from the International Energy Agency, the global FCEV fleet reached around 100,000 units in 2024, with passenger cars dominating the segment [7,8]. Alongside the growing adoption of electric vehicles, refueling infrastructure is also expanding. The number of Hydrogen Refueling Stations (HRSs) nearly doubled between 2020 and 2024, reaching just over 1200 units. To achieve a proper reduction in GHG emissions, however, the hydrogen used in FCEVs must be produced sustainably. The most effective pathway is green hydrogen production through electrolysis powered by renewable sources, which avoids CO_2 emissions associated with fossil-based hydrogen [9]. Indeed, studies have shown that the use of green hydrogen in FCEVs results in significantly lower environmental impacts compared to diesel buses and even to hydrogen derived from natural gas or grid electricity [10].

Building on this perspective, several techno-economic and optimization studies have explored different solutions for green hydrogen infrastructure including HRSs. Genovese et al. investigated a hydrogen infrastructure including a Hydrogen Generator (HG), a Hydrogen Compressor (HC), a storage system, a Pre-Cooling (PC) unit and dispenser, designed to supply green hydrogen to heavy-duty vehicle fleets. Two power supply options were compared: green electricity and direct on-site solar PV. Results showed that solar-powered infrastructures are more cost-effective, with a Levelized Cost of Hydrogen (LCOH) ranging from 5.5 to 27.5 €/kg_{H2} versus 7.4 to 67.8 €/kg_{H2} produced by green electricity [11]. Okonkwo et al. evaluated a hybrid renewable energy system comprising Photovoltaic (PV), Wind Turbine (WT), HG, Battery Storage (BS) and Hydrogen Tanks (HTs) for powering an HRS in Al-Kharj, Saudi Arabia. Using HOMER 3.7 software, they identified an optimal configuration characterized by the smallest component capacity with an LCOH of 9.34 $/kg and a Levelized Cost of Energy (LCOE) of 0.6208 $/kWh, making it the most cost-effective solution for local green hydrogen production [12]. Parsibenehkohal et al. proposed a two-stage optimization framework for coordinating networked microgrids with HRSs and BEV charging stations. The model integrated renewable sources (PV, wind), thermal generators, BS, BEVs, FCEVs, an HRS and an HG, and it was designed to minimize both operational costs and emissions. Results indicated a 4.77% reduction in operating costs and a 49.13% decrease in emissions when using multi-objective optimization [13]. Ancona et al. developed an optimization methodology for hybrid PV/hydrogen microgrids, including PV panels, BS, HG, hydrogen storage and a fuel cell. The model maximized renewable self-consumption and storage efficiency through optimal sizing and management. The optimal configuration included a 3.7 kW HG, 4 kW fuel cell, and 36 kWh BS. The system achieved approximately 30% storage efficiency in summer and 40% in winter, producing 87.5 kg of hydrogen annually [14]. Safak et al. proposed a multi-objective optimization model for a grid-interactive HRS integrating renewable energy sources, BS, HG, a fuel cell and HT. Results demonstrated that renewable integration improves sustainability and enables surplus hydrogen production, thereby reducing external dependence and increasing profitability. The optimal configuration yielded the highest financial gain (587.83$), although the load factor could only be maximized without renewable generators because of trade-offs with grid stability [15]. Sun et al. presented a load management strategy for an HRS comprising an HG, HC and storage to support grid integration of renewable energy produced with WT. By adjusting electricity consumption in real time, the HRS reduced transformer overloading and avoided up to 92% of wind curtailment compared to passive operation. Over one year, this strategy enabled 5.8 GWh of wind energy to be utilized and reduced electricity costs by 7.5%, with an additional 5% savings possible through grid service rewards [16]. Al-Sharafi investigated the techno-socio-economic feasibility of an HRS powered by hybrid PV/WT systems in Saudi Arabia. The system included PV panels, WT, HG, HC, HT, a fuel cell, and cooling/dispensing units. Using real refueling data from four area types, they optimized system sizing for off-grid and on-grid scenarios. Results showed that synchronization between solar availability and hydrogen demand (Social-to-Solar Fraction, STSF) significantly affects cost: the industrial area (STSF = 0.62) achieves the lowest hydrogen cost (7.81–9.62 $/kg), while the tourist area (STSF = 0.38) has the highest (7.81–9.90 $/kg) [17]. Rizk-Allah et al. presented a techno-economic analysis of a standalone wind–PV power plant designed to produce green hydrogen for a refueling station and electricity. The system included PV panels, WT, HG, BS and HTs. Using HOMER pro software, the optimal configuration generates 6,997,990 kWh/year and 85,595 kg/year of hydrogen, with an LCOH of 2.89 €/kg and a net present cost of 5.49 M€ [18]. Di Micco et al. presented a techno-economic analysis of an on-site solar-powered HRS. The system included a PV plant, HG, BS and HCs. The station can produce up to 450 kg/day of green hydrogen, with an annual output of 123.1 t_{H2}. The LCOH was estimated at 10.71 €/kg, with the production section contributing 89% of the total cost [19]. Barhoumi et al. analyzed three PV-based configurations for a green HRS in Salalah, Oman. The authors compared grid-connected PV, stand-alone PV with BS and stand-alone PV with fuel cells. Each system included PV panels, HG, HTs and inverters. The grid-connected PV system produced 58.62 t_{H2} annually at an LCOH of 5.5 €/kg, with the lowest net present cost. The BS and fuel cell systems achieved higher costs (5.74 €/kg and 7.38 €/kg, respectively) but offered zero emissions, while the grid-connected option was identified as the most cost-effective [20]. Bahou performed a techno-economic analysis of an on-site HRS powered by grid-connected PV panels to supply fuel cell taxis. Key components included HG, low- and high-pressure tanks and a solar system. The station was designed to produce up to 152 kg/day of hydrogen. Results showed hydrogen costs ranging from 9.18 to 12.56 $/kg, depending on station size [21]. Hussain et al. developed an optimization model for sizing a stand-alone HRS powered by on-site WT and PV. Key components included WT, PV, HG and hydrogen storage tanks. The station was designed to meet a daily hydrogen demand of 2 t_{H2}/day, scalable to 10 t_{H2}/day. Two configurations were analyzed: near-green (minimal hydrogen import) and mixed-green (up to 18% imported hydrogen). The results showed an LCOH ranging from 2.94 to 8.99 $/kg [22]. Kavadias et al. investigated the sizing and economic viability of an HRS powered by surplus energy from a wind farm in Greece. Economic analysis showed that scenarios with higher FCEV penetration ($\geq$100 vehicles) are financially viable, with payback periods of approximately 7.4–10 years and specific hydrogen costs of 11.5–12.8 €/kg [23]. Gu et al. compared four solar-integrated hydrogen supply routes for refueling stations. The station included HG, storage tanks and HCs. Route IV (on-site solar electrolysis) achieved near-zero CO_2 emissions, while Route III (liquid H_2 delivery) reduced emissions by 96%. Routes III and IV also showed superior energy efficiency, consuming 27% and 38% less energy than coal-based H_2 production [24]. Tang et al. evaluated the economic feasibility of an HRS powered by solar PV and WT in Sweden, comparing on-grid and off-grid configurations. The HRS included HG, solar PV units, WT, and hydrogen storage tanks. Simulations across nine cities showed that wind speed significantly affects hydrogen cost, while solar radiation has less impact. The LCOH ranged from 71 to 153 SEK/kg for off-grid configurations and from 35 to 72 SEK/kg for the on-grid configurations. Combining solar and wind improved performance, while grid integration substantially reduced the LCOH, particularly in low-wind regions [25].

The main results of the previous studies are summarized in Table 1.

Table 1. Studies on hydrogen refueling stations integrated into renewable microgrids.

Reference	PV [kW]	WT [kW]	BS [kWh]	HG [kW]	HS Capacity [kg]	HS Pressure [MPa]
[11]	1000	-	-	1000	400	3–70
[12]	270–520	300–600	70–100	500–800	100	
[13]	100–750	400–2300	-	-	-	-
[14]	11.4	-	36	3.7	87.5	-
[15]	500	1000	1000	500	1000	-
[16]	-	1000	-	2900	440	-
[17]	88–419	600	-	240	50–830	35–70
[18]	298	2200	600	1000	800	-
[19]	8000	-	3500	2100	450	200–900
[20]	3000–4000	-	-	1000	300	
[21]	1944	-	-	453.5	0.9–47.7	0.5–87.5
[22]	22,000	18,000	-	11,000–14,000	11,700	70
[23]		10,000	-	8000	2295.1	70
[24]	-	-	-	-	500	45
[25]	250	250	-	270	1900	-

Previous studies on HRSs can be grouped into techno-economic analyses of renewable-powered systems, optimization frameworks for integration into energy systems and microgrids, and operational strategies such as load management and grid interaction. However, many studies do not specify key parameters such as hydrogen dispensing pressure or production capacity and often focus on hydrogen cost and production rather than the operational management of the station itself. These limitations reduce the practical applicability of HRS integration, where safety standards, refueling protocols, and user requirements are also critical.

In response to these gaps, this study proposes an integrated approach that bridges hydrogen refueling infrastructure modeling with renewable microgrid optimization, addressing both technical performance and techno-economic feasibility. A detailed mathematical model was developed in MATLAB 2023b to evaluate the performance of a renewable-based microgrid integrated with an HRS under different Energy Management Strategies (EMSs), characterized by different shares of green hydrogen production.

In particular, two different EMSs were considered: a fully renewable-based hydrogen production strategy (GREEN-EMS), where hydrogen is produced exclusively using renewable electricity, and a mixed strategy (MIXED-EMS), in which hydrogen production is supplied by both renewable and grid electricity. A third strategy based exclusively on grid electricity (GRID-EMS) was included as a reference case. All the EMSs explicitly incorporate the operational constraints mentioned above, ensuring that hydrogen production, storage, and dispensing are consistent with realistic station operation, including demand-driven refueling behavior and system-level operational limits.

The microgrid configuration was optimized to determine the optimal component sizes according to two objective functions: maximizing the Self-Sufficiency Rate (SSR) and minimizing the Levelized Cost of Hydrogen (LCOH). The LCOH analysis quantifies the additional costs associated with integrating energy storage systems to support green hydrogen production compared with the costs of operating the electrolyzer exclusively using grid electricity. Additionally, a comprehensive cost analysis accounts for revenues from surplus electricity sales and the expected future reduction in HG costs. Finally, the avoided CO_2 emissions are quantified for each EMS considering emissions associated with electricity consumption for hydrogen production and HRS operation. It should be noted that the overall environmental performance of hydrogen mobility also depends on vehicle-side PEM fuel cell operation, as appropriate water-content regulation and purge control can improve hydrogen utilization, reduce auxiliary energy consumption, and enhance fuel cell durability [26].

To simulate a realistic hydrogen demand, the model is based on an urban bus fleet operating in Cagliari (Italy), where the service is currently provided by diesel buses and is being considered for conversion to FCEVs. The bus line characteristics, including route length, operating speed, and fleet size, are used to derive hydrogen consumption profiles and a daily refueling schedule.

The specific objectives of this study are:

- To integrate an HRS into a renewable microgrid and optimize the system design using a multi-objective approach that minimizes the LCOH while maximizing the SSR;
- To evaluate the techno-economic feasibility and environmental sustainability of renewable hydrogen infrastructure by comparing different EMSs, assessing the economic impact of grid interaction and surplus energy sales, and quantifying the environmental impact through a CO_2 emissions analysis of the different hydrogen-production pathways.

2. Materials and Methods

In the following, the system configuration considered in this study is presented. Subsequently, an overview of the mathematical modeling of the system components is provided. Finally, the management strategies considered in this study are described and discussed together with the main characteristics of the optimization approach adopted.

2.1. System Configuration

The renewable microgrid configuration considered in this study is shown in Figure 1. It includes a PV system coupled with a BS and a hydrogen production, storage and utilization system, consisting of a Hydrogen Generator (HG), a Low-Pressure Tank (LPT), a Hydrogen Compressor (HC), a Pre-Cooling (PC) unit, a cascade system of High-Pressure Tanks (HPTs) and vehicle tanks (VTs). A connection to the Public Grid (PG) is optionally included to investigate two different EMSs, characterized by an increasing share of renewable energy used for green hydrogen production, as already explained above. The figure also shows how all the components that require electrical energy (HG, HC, and PCs) are supplied. Specifically, electrical power is provided by the PV system, BS, or, when necessary, the PG.

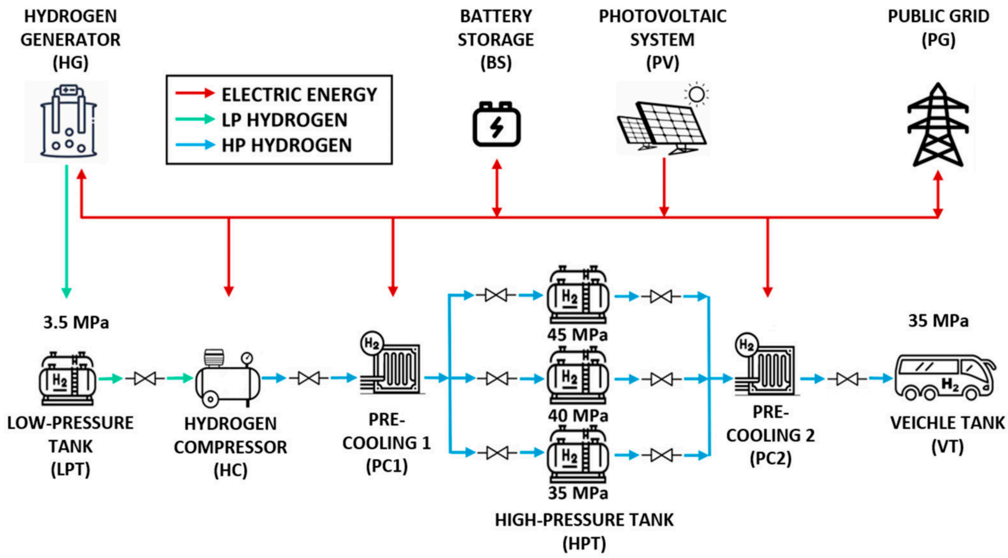

Figure 1. Schematic of the HRS integrated into the renewable-based microgrid.

The HRS is designed to supply green hydrogen to a fleet of 21 buses. As reported in Table 2, the selected bus has a driving range of 500 km and is equipped with 6 tanks capable of storing 35 kg of hydrogen at 35 MPa. The route considered has a round-trip distance of 24.3 km, with an average operating speed of 13.3 km/h. Accordingly, each bus consumes 1.7 kg per complete round trip, corresponding to 0.931 kg per operating hour (since a round trip takes approximately 1 h and 50 min). The specific CO_2 emissions reported by the local bus operator are 1.072 kg CO_2/km [27]. Consequently, considering the total distance of the line over the year, the CO_2 emissions associated with the existing diesel buses amount to approximately 1.50 kt CO_2/year.

Table 2. Bus line route and hydrogen bus characteristics [28].

Parameter		Value	Parameter		Value
Route round-trip distance	[km]	24.3	Bus autonomy	[km]	500
Average operating speed	[km/h]	13.3	Bus tank pressure	[MPa]	35
Daily line distance	[km/day]	3828	Bus total capacity	[kg]	35
Refueling time	[s]	109.6	Number of bus tanks	[-]	6
Max buses in service	[-]	21	H_2 consumption	[kg/RT]	1.7
				[kg/h]	0.931

Starting from the daily hydrogen demand, the annual hydrogen demand of the HRS was determined, assuming that the buses operate every day of the year. This assumption allows a consistent annual hydrogen-demand profile to be generated without introducing uncertainties associated with holidays, service interruptions, or seasonal timetable variations and represents a conservative scenario in terms of annual HRS demand.

Based on the season-dependent energy consumption of the HRS components, an hourly electrical-demand profile was generated for the entire year. The annual hydrogen demand of the HRS amounts to 100.25 t/year (equivalent to 3948.2 MWh/year), while the total annual energy consumption of the HRS (HC and two PCs) is 178.67 MWh/year.

2.2. Mathematical Models

The mathematical models used to evaluate the expected performance of each component of the considered renewable microgrid are described below.

2.2.1. PV System

The PV generation profile was simulated using a typical meteorological year dataset of the location considered, Cagliari (Italy), obtained from Meteonorm [29]. The PV system consists of modules with a peak power of 355 W [30], while the nominal PV power ($P_{PV,NOM}$) is considered a design parameter to be optimized. Regarding the PV plant orientation, an azimuth angle of −30° and a tilt angle of 30° were considered. The output power P_{PV} of the PV subarray was calculated using Equation (1):

$$P_{PV}(t) = P_{PV,NOM} \frac{GI(t)}{GI_{STC}} \left[1 + \gamma \left(T_C(t) - T_{C,STC}\right)\right] \eta_{INV}\, f_{PV} \tag{1}$$

where the reference irradiance (GI_{STC}) was set to 1000 W/m^2, the PV cell temperature at Standard Test Conditions $\left(T_{C,\,STC}\right)$ was set to 25 °C, the PV temperature coefficient (γ) was −0.35%/K, while the inverter efficiency (η_{INV}) was given by the manufacturer as a function of the PV power output. Secondary losses, including wiring losses, shading, soiling of the modules and aging, were accounted for through a derating factor f_{PV} of 0.9. The Global Irradiance (GI) and the operating Cell Temperature $\left(T_C\right)$ were calculated using the method proposed by Duffie and Beckman [31]. Specifically, the operating cell temperature T_C of the PV module was calculated using Equation (2):

$$T_C(\mathrm{t}) = \frac{T_A(\mathrm{t}) + (T_{NOCT} - T_{A,NOCT})\frac{GI(t)}{GI_{NOCT}}\frac{U_{PV,NOCT}}{U_{PV}}\left[1 - \eta_{PV,NOM}\frac{1-\gamma\,(T_{C,STC}+273.15)}{\tau\alpha}\right]}{1 + (T_{NOCT} - T_{A,NOCT})\,\frac{GI(t)}{GI_{NOCT}}\,\frac{\eta_{PV,NOM}\cdot\gamma}{\tau\alpha}} \tag{2}$$

where T_{NOCT} is the Nominal Operating Cell Temperature (NOCT, temperature of the cell without any load), with an incident radiation GI_{NOCT} of 800 W/m^2 and an ambient temperature $T_{A,NOCT}$ of 20 °C; U_{PV} and $U_{PV,NOCT}$ are the heat transfer coefficients at the effective and NOCT conditions, respectively; $\eta_{PV,NOM}$ is the nominal PV efficiency, and $\tau\alpha$ is the transmittance–absorption coefficient (assumed equal to 0.9). The actual PV efficiency η_{PV} was then calculated using Equation (3):

$$\eta_{PV}(t) = \eta_{PV,NOM}\,[1 + \gamma\,(T_C(t) - T_{C,STC})] \tag{3}$$

Table 3 summarizes the main characteristics of the PV modules considered.

Table 3. Main characteristics of the PV module considered [30].

Parameter	Value
PV module power at standard test conditions	355 W
PV nominal operating cell temperature (T_{NOCT})	45 °C
PV nominal efficiency ($\eta_{PV,NOM}$)	20.6%
PV module active area (AA_{MOD})	1.72 m^2
PV temperature coefficient (γ)	−0.35%/K
PV derating factor (f_{PV})	0.9
Inverter efficiency (η_{INV})	90–97.8%

2.2.2. Battery Storage

The battery storage system was represented using a simplified energy-balance model with constant charging and discharging efficiencies, while battery degradation, temperature effects, and rate-dependent behavior were not explicitly modeled. This formulation was selected to limit the computational burden associated with the multi-objective optimization. The energy stored in the battery bank was evaluated through its state-of-charge, SOC_{BS}, defined as the ratio between the stored energy and the nominal storage capacity and calculated using Equation (4):

$$SOC_{BS}(t+1) = SOC_{BS}(t) + \frac{\left(P_{BS,c}(t)\,\eta_{BS,c} - \frac{P_{BS,d}(t)}{\eta_{BS,d}}\right)\Delta t}{E_{BS}} \tag{4}$$

where $P_{BS,c}$ is the power input during the charging phase and $P_{BS,d}$ is the power output during the discharging phase. The batteries charging and discharging efficiencies ($\eta_{BS,c}$ and $\eta_{BS,d}$) were set equal to 98% and 97%, respectively, consistent with the assumed lithium-ion battery technology, while the applied time step (Δt) and the battery Depth-of-Discharge (DOD_{BS}) were assumed equal to 1 h and 80%, respectively [32]. The nominal battery capacity (E_{BS}) was considered a design parameter to be optimized.

2.2.3. Hydrogen Section

The hydrogen section includes an HG and an LPT, in which hydrogen is stored up to the HG delivery pressure (while the minimum pressure is set equal to 1.5 MPa, equal to the minimum working pressure of the HC as previously explained). The nominal power of the HG and the capacity of the LPT were considered optimization variables.

A commercial electrolyzer based on the Proton Exchange Membrane (PEM) technology, with a hydrogen production of 1 Nm^3/h at 35 bar(g), was used as the reference unit for defining the specific energy consumption, efficiency curve, and operating range of the hydrogen generator. The optimized MW-scale capacities were obtained by considering the modular scale-up of the electrolyzer system through an increase in the number of cells per stack and the number of stacks operating in parallel. At the system level, the scaled units were assumed to retain the normalized efficiency and part-load characteristics of the reference electrolyzer, while the total power consumption and hydrogen production capacity were assumed to increase proportionally with the installed capacity. According to the manufacturer's specifications [32], it was assumed that the HG can operate between 20% and 100% of its rated power. The HG frequently operates under part-load conditions because the available PV power and HRS demand vary over time. Therefore, the hydrogen mass flow rate produced by the HG $\dot{m}_{HG}$ was calculated as a function of the power supply P_{HG} and the electrolyzer efficiency η_{HG} [32], using Equation (5):

$$\dot{m}_{HG}(t) = \frac{\eta_{HG}(t) \cdot P_{HG}(t)}{HHV_{H_2}} \tag{5}$$

where HHV_{H_2} is the Higher Heating Value of the hydrogen.

Finally, the energy stored in the LPT at a given time was evaluated based on the Level of Hydrogen (LOH), determined by Equation (6):

$$LOH_{LPT}(t+1) = LOH_{LPT}(t) + \frac{\left[\dot{m}_{HG}(t) - \dot{m}_{HC}(t)\right] HHV_{H_2} \cdot \Delta t}{E_{LPT}} \tag{6}$$

where $\dot{m}_{HC}$ is the hydrogen mass flow rate compressed by the HC, while E_{LPT} is the hydrogen storage capacity expressed in energy terms of the LPT.

2.2.4. Energy Management Strategies

To evaluate the performance of the renewable microgrid under increasing shares of green hydrogen production, three different Energy Management Strategies (EMSs) were developed and investigated.

The first strategy, referred to as the GREEN-EMS, is illustrated in Figure 2. The black section represents the control logic governing hydrogen production using the PV and/or BS, while the green section describes how the HRS demand is supplied by the LPT. Each logic node and its corresponding control action are identified by matching colors. Specifically, the yellow node determines the electrical power available for hydrogen production, calculated as the PV generation minus the power consumption of the HRS components (mainly HCs and PCs). If the available energy exceeds the minimum required by the HG, a check on the LPT (orange node) is performed to decide whether hydrogen should be produced under nominal or partial load conditions (pink node). When hydrogen production is possible but the LPT has insufficient free capacity, the surplus PV electricity, after supplying HRS components, is directed to the BS or, if the batteries are fully charged, exported to the grid (light blue node). Conversely, if the available energy is insufficient to operate the HG at its minimum load, a check on the SOC_{BS} is carried out to determine whether the HG can be supplied with electricity from both PV and BS (blue node). When sufficient storage capacity is available in the LPT, hydrogen is produced at either intermediate or nominal load (brown node). Otherwise, the surplus PV electricity is exported to the grid. Regarding hydrogen demand from the HRS (pink node, green section), if the LPT cannot fully satisfy the required demand, it supplies the available hydrogen until its minimum allowable storage level is reached (grey node).

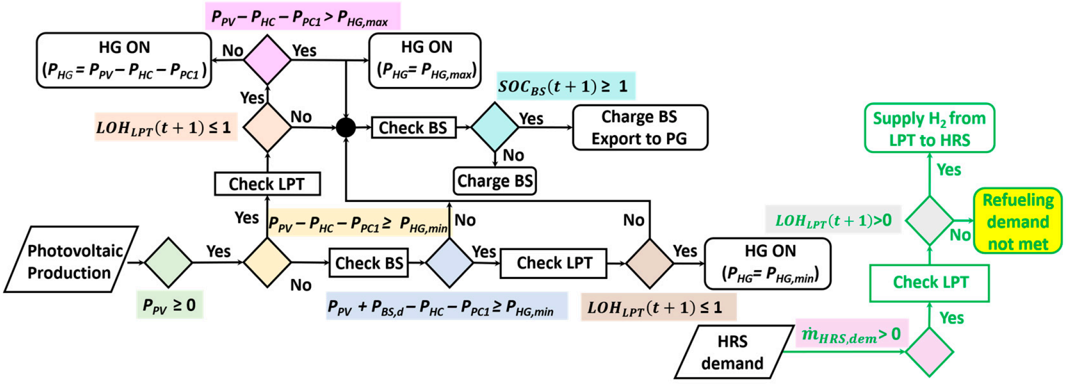

Figure 2. Energy management strategy scheme of the GREEN-EMS.

The MIXED-EMS is illustrated in Figure 3. The black section, representing hydrogen production using PV and BS electricity, and the green section, representing hydrogen supply to the HRS, are identical to those of the GREEN-EMS. The main difference is the red section, which represents hydrogen production using electricity from the grid when the hydrogen expected to be available is insufficient to meet the upcoming HRS demand. Specifically, when the HRS requires hydrogen (dark grey node), a check on the LPT is performed five hours before the scheduled refueling time (dark green node). If the amount of hydrogen available, considering both the current storage level and the quantity expected to be produced in the next five hours using PV and BS electricity, is lower than the HRS demand (violet node), the deficit is compensated by producing hydrogen using electricity from the grid (light yellow node). This five-hour predictive horizon corresponds approximately to the time required for the MW-scale HG, operating at nominal load, to produce the hydrogen needed to satisfy the expected bus-refueling demand.

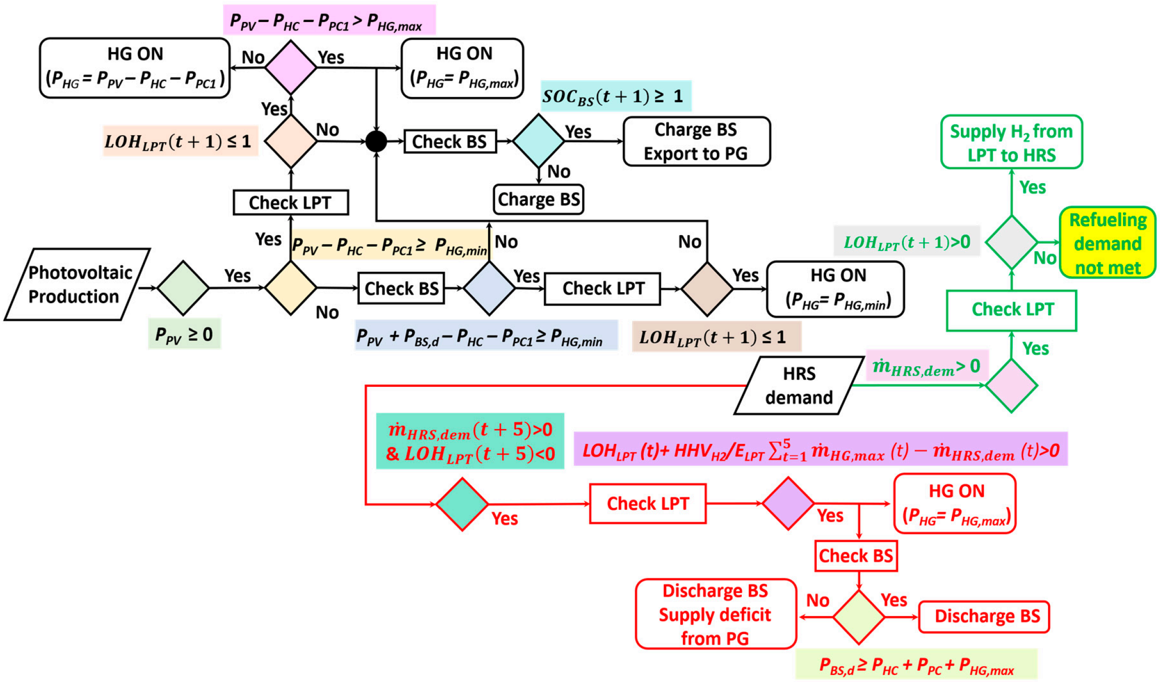

Figure 3. Energy management strategy scheme of the MIXED-EMS.

The two proposed EMSs were also compared with a GRID-EMS, in which hydrogen is produced exclusively using electricity from the grid. The GRID-EMS follows the grid-assisted section of the MIXED-EMS but excludes the PV and BS control logic because these components are not included. Consequently, the HG can operate throughout the day using electricity supplied by the PG.

2.2.5. Microgrid Optimization Settings

A multi-objective optimization is formulated and solved with the goal of finding the optimal design of the renewable-based microgrid by considering two conflicting objective functions: the maximization of the Self-Sufficiency Rate (SSR) and the minimization of the Levelized Cost of Hydrogen (LCOH). The first objective represents the ability of the microgrid to satisfy the HRS demand using green hydrogen, and it is defined as the ratio between the annual amount of green hydrogen produced by the HG, $m_{HG,green}$, and the total annual hydrogen demand of the HRS, $m_{HRS,dem}$ (Equation (7)). The second objective represents the average total cost of delivering one kilogram of hydrogen by the HRS over the entire life cycle (Equation (8)).

$$\mathrm{SSR} = \frac{m_{HG,green}}{m_{HRS,dem}} \tag{7}$$

$$\mathrm{LCOH} = \frac{TCI + (E_{FG} \cdot c_{FG} + OM \cdot TCI) \cdot \sum (1+IR)^{-y}}{m_{HRS,del} \cdot \sum (1+IR)^{-y}} \tag{8}$$

where TCI is the total capital investment, c_{FG} indicates the specific cost for the energy purchased from the grid multiplied by the total quantity of energy purchased (E_{FG}), OM represents the Operating and Maintenance costs, IR is the Interest Rate, y is the total lifetime, and $m_{HRS,del}$ denotes the actual annual mass of hydrogen delivered by the HRS (which can differ from $m_{HRS,dem}$, as may occur under the GREEN-EMS). The terms E_{FG}, OM and $m_{HRS,del}$ were assumed to remain constant over the project lifetime.

Regarding Equation (8), it can be observed that, while the cost of purchasing electricity from the grid has been included through the term E_{FG}, the revenue from selling surplus renewable energy has instead been excluded. This choice was made because including electricity-sales revenue during optimization could lead to excessive oversizing of the PV system to maximize exports and artificially reduce the LCOH. Such a configuration would not be consistent with the principal purpose of the system, namely the production and delivery of hydrogen to the HRS. Electricity-export revenues were therefore evaluated separately after the optimization. The total capital investment is calculated using Equation (9), starting from the Purchase Equipment Costs (PEC) as a function of the relative size of the hydrogen section components and their cost parameters c (listed in Table 4):

$$\begin{aligned} TCI = \Big(& c_{PV} \cdot P_{PV} + c_{BS} \cdot \tfrac{E_{BS}}{DOD_{BS}} + c_{HG} \cdot P_{HG}{}^{0.885} + c_{LPT} \cdot m_{LPT} + \textstyle\sum_{i=1}^{3} c_{HPT,i} \cdot m_{HPT,i} \\ & + c_{HC} \cdot P_{HC}{}^{0.4603} + c_{PC1} \cdot P_{PC1} + c_{HRS} \Big) (1 + c_{BOP})(1 + c_{EC}) \end{aligned} \tag{9}$$

where c_{BOP} denotes the Balance-Of-Plant (BOP) cost, expressed as a percentage of the PEC, while c_{EC} denotes the engineering cost, expressed as a percentage of the sum of PEC and BOP costs. All power and energy terms refer to the nominal size of the corresponding component. The parameter c_{BS} represents the aggregate specific investment cost of the battery storage system, including the battery modules, power conversion system, and replacement costs over the 20-year project lifetime. The parameters c_{HG} and c_{HC} are the coefficients used in the nonlinear investment-cost correlations for the hydrogen generator and hydrogen compressor, respectively. c_{HG} also includes the power electronics and balance-of-plant costs for the HG, the water-treatment equipment and associated costs required to supply high-purity water for electrolysis, and electrolyzer-stack replacement during the project lifetime. All other major components were assumed to have a service life equal to the 20-year project horizon. Consequently, no replacement costs were considered for these components, and a zero residual value was assumed for the entire system at the end of the project lifetime.

Table 4. Main parameters assumed for the economic analysis [32–36].

Parameter		Value	Parameter		Value
y	[year]	20	c_{HC}	[€ kW$^{-0.4603}$]	55,350
OM	[%]	5% TCI	c_{HPT}	[€/kg]	1390.35
IR	[%]	5	c_{PC1}	[€/kW]	500.77
c_{BOP}	[%]	10% PEC	c_{HRS}	[€]	158,100
c_{EC}	[%]	10	m_{HPT1}	[kg]	59
c_{FC}	[€/kWh]	0.114	m_{HPT2}	[kg]	63.5
c_{PV}	[€/kW]	1058.34	m_{HPT3}	[kg]	64
c_{BS}	[€/kWh]	697.5	P_{HC}	[kW]	400
c_{HG}	[€ kW$^{-0.885}$]	3165.72	P_{PC1}	[kW]	5
c_{LPT}	[€/kg]	930.93			

Table 4 also reports the nominal hydrogen capacity of the cascade storage system and the nominal powers of the HC and the upstream pre-cooling unit (PC1). The cost of the downstream pre-cooling unit (PC2) is included in the aggregate HRS cost.

The two objectives are inherently conflicting. Increasing the SSR typically requires oversizing renewable and storage components, which raises investment and operational costs, thus leading to a higher LCOH. Conversely, minimizing the LCOH often results in a smaller renewable share and higher grid dependence, thereby lowering the SSR. Therefore, the optimization problem cannot yield a single global optimum but rather a set of non-dominated solutions that represent the trade-off between autonomy and cost. The resulting Pareto front provides a range of feasible configurations, from the most cost-effective to the most self-sufficient. A final configuration can therefore be selected according to the technical and economic priorities of the decision maker, including minimum-LCOH, maximum-SSR, or balanced solutions.

The optimization problem is implemented in MATLAB and solved using the Non-Dominated Sorting Genetic Algorithm II (NSGA-II) [37]. A population of 2000 individuals was defined to ensure a wide exploration of the design space. The optimization stopped when the default convergence criteria were met, either when the maximum number of generations (by default, 100 times the number of variables) was reached or when improvement of the Pareto front over consecutive generations (default function tolerance was 10^{-4}) became negligible. All other genetic operators were kept at MATLAB default settings:

- Selection method: tournament selection (default selection pressure = 0.75);
- Crossover operator: scattered crossover (default crossover fraction = 0.8);
- Mutation function: adaptive feasible mutation;
- Pareto ranking and elitism: controlled elitist strategy inherent to NSGA-II.

This configuration provided balancing between exploration of the design space and convergence toward the non-dominated optimal solutions. The design variables to be optimized and the corresponding lower and upper bounds are:

- PV plant nominal power: 2000–10,000 kW;
- BS nominal capacity: 100–5000 kWh;
- HG nominal power: 1000–3000 kW;
- LPT geometric volume: 50–500 m^3.

These bounds were defined through preliminary screening of the design space to limit the generation of infeasible or unrealistic candidate solutions while preserving a sufficiently broad range of potential configurations. The lower bounds exclude configurations unable to satisfy the hydrogen demand or the minimum operating constraints of the components, whereas the upper bounds allow the exploration of highly renewable and self-sufficient configurations without unnecessarily enlarging the optimization domain.

3. Results and Discussion

The annual performance of the renewable microgrid under the different EMSs is presented and discussed in this section. The results, represented by the Pareto fronts obtained from the multi-objective optimization, are also compared with the hydrogen production costs resulting from powering the HG exclusively with electricity from the public grid, highlighting the additional costs arising from the need for storage systems to guarantee the production and use of green hydrogen.

3.1. Results of the GREEN-EMS

This section presents the results obtained using the GREEN-EMS. The Pareto front and the variation in the sizes of the microgrid components for all points along the Pareto front, corresponding to increasing values of the SSR, are shown in Figures 4 and 5, respectively.

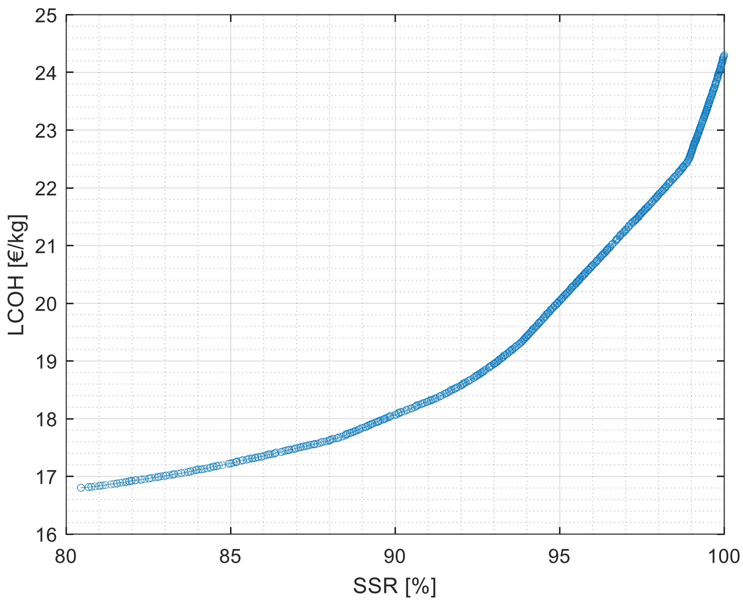

Figure 4. Pareto front obtained for the GREEN-EMS case.

The shape of the Pareto front shows the conflict between the two outcomes: lower LCOH values (16.8 €/kg) result in a lower self-sufficiency rate (80.44%), while higher costs (24.3 €/kg) must be accepted to achieve an SSR of 100%.

Concerning the component sizes shown in Figure 5, all parameter values lie between the lowest and highest values of the two objective functions. As can be seen, achieving a 100% SSR requires larger component sizes: both the PV system and the HG exhibit a nearly linear increase in their nominal powers. A general increase in the LPT volume is also observed, although this trend appears somewhat discontinuous, whereas the BS capacity remains almost unchanged.

As shown above, the lowest LCOH, equal to 16.8 €/kg, is obtained for the configuration with the lowest SSR of 80.44%, whereas achieving an SSR of 100% results in an increase in the LCOH to 24.3 €/kg. This rise in hydrogen production cost can be explained by comparing the design variables associated with these two extreme configurations:

- Lowest LCOH: PV = 3978 kW; BS = 198 kWh; HG = 1917 kW; LPT = 128 m^3;
- Highest SSR: PV = 8398 kW; BS = 384 kWh; HG = 2909 kW; LPT = 462 m^3.

As can be observed, all components increase in size. In particular, the PV capacity slightly more than doubles, the BS capacity nearly doubles, and the LPT volume more than triples, while the HG increases to a lesser extent. The increase in the SSR is mainly achieved through the significant expansion of the PV capacity, which roughly doubles when comparing the two extreme cases (lowest LCOH vs. highest SSR). The larger PV field enables a greater amount of renewable energy generation, thus improving system autonomy but also leading to a greater surplus of electricity exported to the grid. In all configurations, the battery storage capacity remains relatively small compared with the PV size, indicating a marginal role in the overall system operation, as it mainly serves to smooth short-term fluctuations rather than providing large-scale energy shifting. An interesting trend can also be observed in the ratio between the HG and PV nominal powers, which decreases from approximately 0.5 in the lowest-LCOH case to around one-third in the highest-SSR configuration. This suggests that the improvement in the SSR is primarily due to the increased renewable capacity and the consequently longer operating hours of the electrolyzer, rather than to a direct enlargement of the HG itself. However, this also implies a greater amount of surplus PV production that is sold to the grid, which is addressed in the following discussion on system energy balance and economic implications.

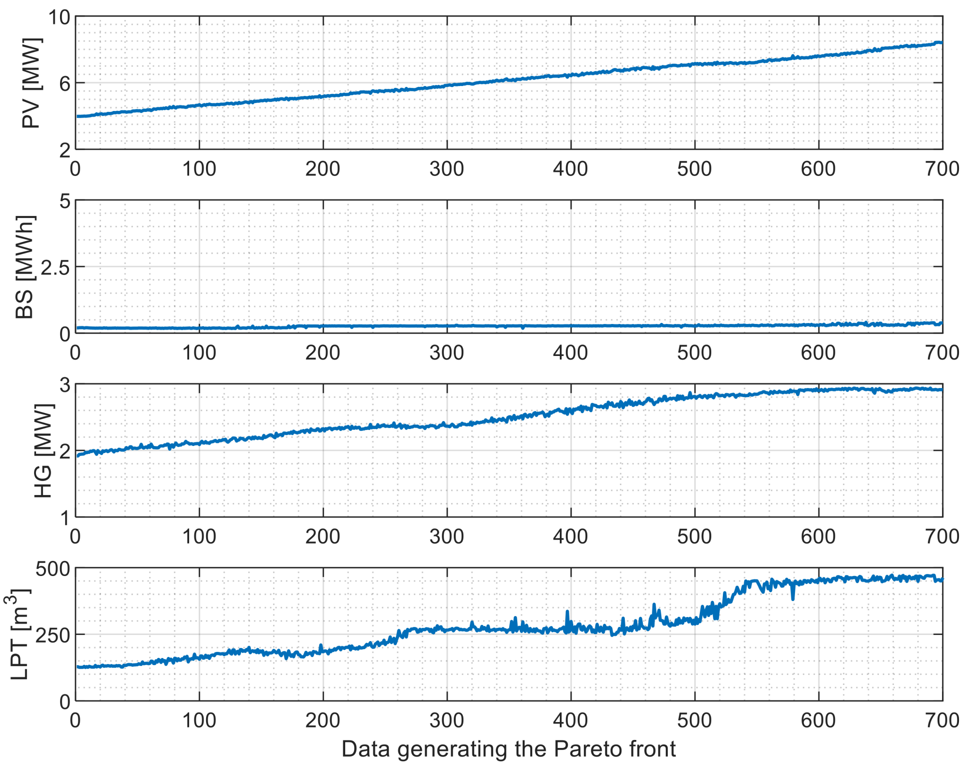

Figure 5. Sizing of renewable-based microgrid components (GREEN-EMS).

Since the possible revenue from electricity exported to the grid was excluded during the optimization process, the resulting LCOH value was subsequently corrected, as indicated in Equation (10):

$$\mathrm{LCOH}' = \mathrm{LCOH} - \frac{E_{TG} \cdot c_{TG}}{m_{HRS}} \tag{10}$$

where LCOH′ represents the hydrogen production cost corrected by subtracting the revenue from electricity sales, calculated as the product of the total amount of energy sent to the grid (E_{TG}) and the electricity selling price (c_{TG}). Starting from the optimized sizes of the microgrid components, the total quantity of energy exported to the grid and the amount of hydrogen actually dispensed were calculated. To evaluate the effect of electricity sales on the hydrogen production cost, three constant electricity selling prices of 0.05, 0.10, and 0.15 €/kWh were considered. These values were selected as representative of typical electricity selling price levels for renewable energy systems in Italy, being close to the guaranteed minimum price [38], the average local market price [39], and the national average price reported for the Italian electricity market in 2025 [38], respectively. Assuming constant selling prices allows the influence of electricity export revenues on the LCOH to be assessed without introducing the variability associated with time-dependent market prices.

The corrected LCOH results, obtained by applying the three electricity price values reported above to Equation (10) through the term $c_{E,TG}$, are shown in Figure 6.

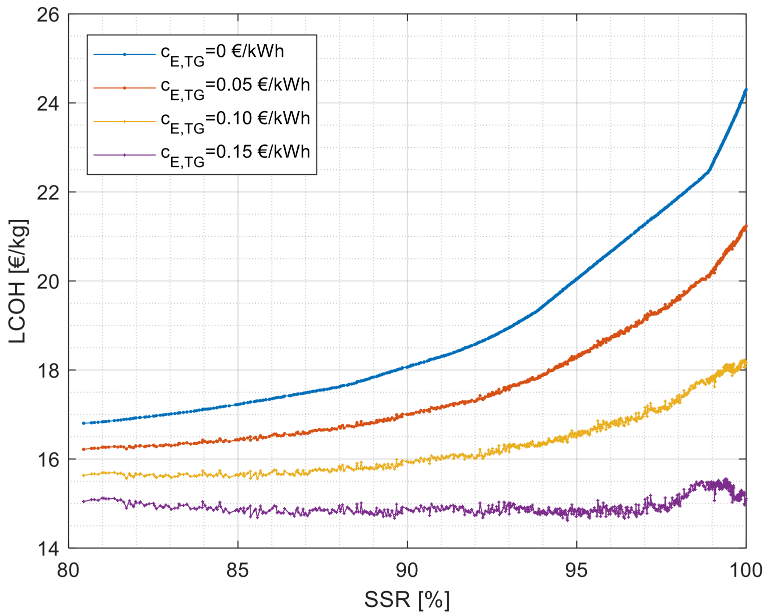

Figure 6. Pareto fronts resulting after LCOH correction (GREEN-EMS).

Specifically, the curve corresponding to the LCOH calculated without considering any potential revenue from selling surplus renewable energy to the grid (illustrated in Figure 4) is represented by the blue line.

As expected from Equation (10), selling the surplus renewable electricity results in a decrease in the overall hydrogen production cost. Moreover, the purple curve, associated with the highest electricity selling price (0.15 €/kWh), exhibits a less uniform progression of LCOH values along the SSR range. This trend is due to the relationship expressed in Equation (10): as the electricity selling price increases, the revenue term increases, thus lowering the costs. Graphically, this result is shown by the greater separation between the points on the curves as the revenue increases.

The minimum costs obtained (corresponding to an SSR of 80.44% for all cases) range between 15.04 €/kg and 16.8 €/kg. The maximum values reach 17.98 €/kg for an electricity selling price of 0.10 €/kWh, close to the Sardinian weighted average electricity price, and 14.92 €/kg when considering the highest electricity selling price, close to the national average price for the first quarter of 2025. Regarding the energy exported to the grid, the annual value varies from 945,841 kWh/year (minimum LCOH configuration) to 6,138,025 kWh/year (maximum SSR configuration).

3.2. Results of the MIXED-EMS

Figure 7 shows the increase in component sizes obtained from the optimization of the MIXED-EMS, corresponding to the points along the Pareto front shown in Figure 8. It should be noted that the SSR considered in this case refers only to green hydrogen production: the overall hydrogen demand is always fully satisfied since hydrogen production from grid electricity is allowed when renewable hydrogen production is insufficient. As previously observed, the PV and HG sizes exhibit a steady increase, while the LPT volume also grows but in a more discontinuous manner. The BS capacity, on the other hand, remains close to its lower limit, consistent with earlier findings.

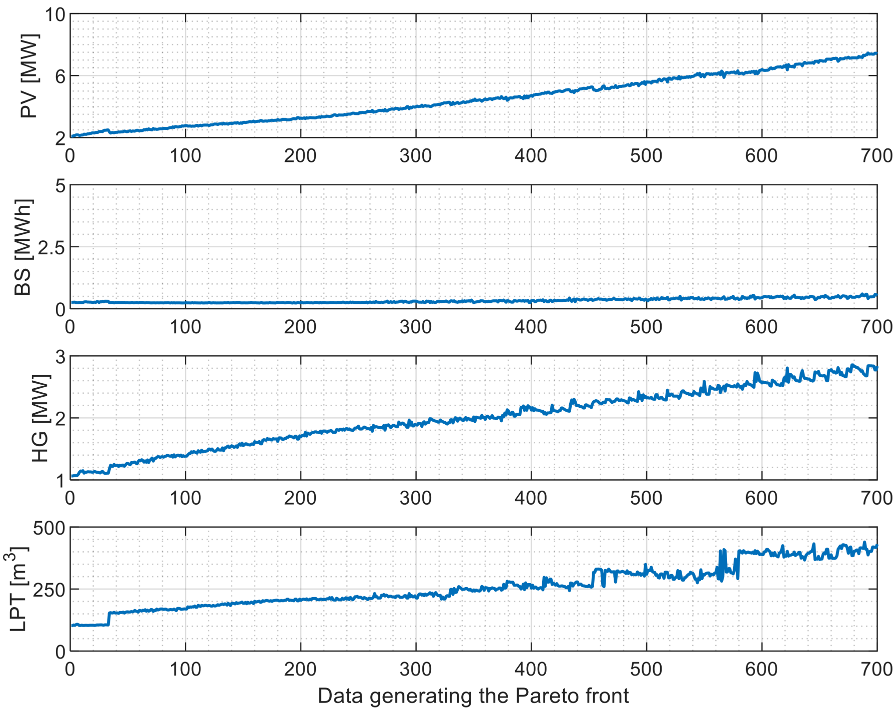

Figure 7. Sizing of renewable-based microgrid components (MIXED-EMS).

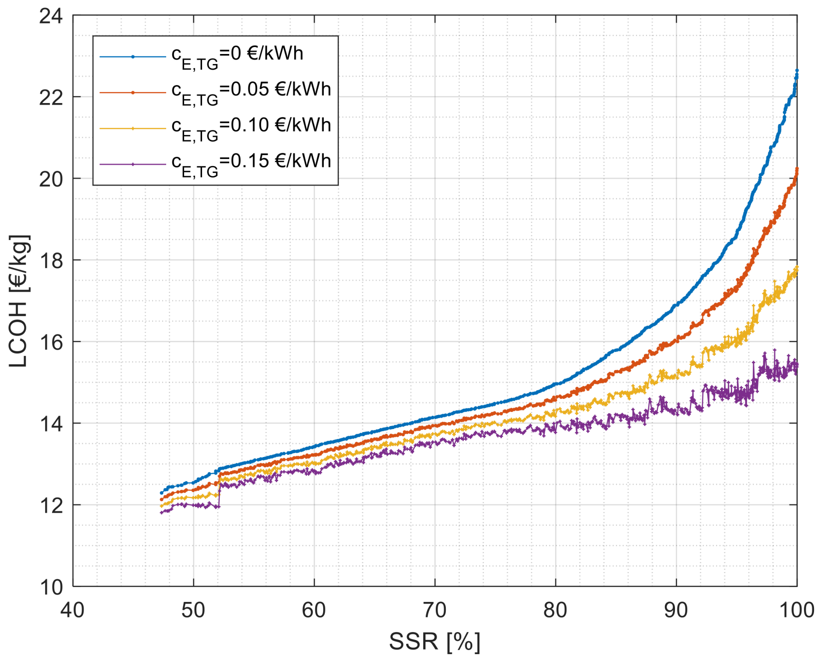

Figure 8. Pareto fronts obtained for the MIXED-EMS with and without LCOH corrections.

In this case, the SSR values are characterized by a wider range than those of the fully renewable configuration. In particular, the microgrid configuration achieving the lowest LCOH (12.29 €/kg, without selling the surplus energy) is characterized by a low SSR (47.34%): this means less than half of the hydrogen is produced using renewable electricity. By contrast, an SSR of 100% results in an LCOH of 22.68 €/kg, slightly lower than that obtained for the GREEN-EMS (24.3 €/kg). The sizes of the components for these two extreme cases are:

- Lowest LCOH: PV = 2088 kW; BS = 258 kWh; HG = 1064 kW; LPT= 103 m^3;
- Highest SSR: PV = 7408 kW; BS = 530 kWh; HG = 2835 kW; LPT = 431 m^3.

The differences in size are evident for all components, with the PV and LPT more than tripling, while the BS and HG approximately double. This behavior can be explained by the system's operating logic: achieving higher SSR values primarily requires increasing renewable generation capacity and hydrogen storage to reduce grid dependence and allow continuous hydrogen production. Conversely, battery capacity plays a secondary role, being used mainly for short-term power balancing rather than large-scale energy shifting, while the HG increases more moderately because the electrolyzer is operated for progressively longer periods rather than being significantly upsized.

Compared with the GREEN-EMS, the MIXED-EMS exhibits overall smaller component sizes for both the lowest-LCOH and highest-SSR solutions. This is due to the additional flexibility provided by the grid connection, which compensates for renewable intermittency without requiring such large PV or storage capacities. However, the relative trends remain consistent: PV and LPT still dominate the capacity increase as the SSR rises, confirming that renewable overgeneration and hydrogen storage expansion are the main drivers for improving system self-sufficiency, albeit at the expense of a higher hydrogen production cost. As in the previous case, the LCOH results were corrected using Equation (10), and the corresponding outcomes are shown in Figure 8.

Unlike the GREEN-EMS, the curves representing the corrected LCOH values show a smaller downward shift. This behavior can be explained by the fact that, except for a few initial points, the amount of hydrogen supplied to the HRS is almost always equal to the total demand. Consequently, the denominator of the equation remains constant, unlike in the previous case in which it increased with the SSR. The minimum costs obtained (corresponding to an SSR of 47.34% for all cases) range between 11.81 €/kg and 12.29 €/kg. The maximum values reach 17.93 €/kg for an electricity selling price of 0.10 €/kWh, close to the local weighted average electricity price, and 15.56 €/kg when considering the highest electricity selling price, close to the national average price for the first quarter of 2025. Regarding the energy exported to the grid, the annual value varies from 322,545 kWh/year (minimum LCOH configuration) to 4,759,973 kWh/year (maximum SSR configuration). In summary, the results obtained after the LCOH correction, considering the sale of surplus energy to the grid, are reported in Table 5.

Table 5. Summary of LCOH and LCOH' for GREEN-EMS and MIXED-EMS (SSR = 100%).

	$c_{E,TG}$ [€/kWh]				
	0	**0.05**	**0.10**	**0.15**	
	LCOH [€/kg]	**LCOH' [€/kg]**	**LCOH' [€/kg]**	**LCOH' [€/kg]**	**SSR [%]**
GREEN-EMS	24.30	21.04	17.98	14.92	100
MIXED-EMS	22.68	20.31	17.93	15.56	100

While Table 5 shows significant cost reductions through energy sales, the absolute LCOH values remain considerably high. To identify the main cost drivers and under-stand how the system configuration changes between different optimization objectives, Figures 9 and 10 present the breakdown of the Total Capital Investment (TCI) for both GREEN- and MIXED-EMS configurations, considering the lowest LCOH and the highest SSR, respectively. It should be noted that cost contributions accounting for less than 1% of the total investment are not visible in the figures because of their negligible impact on the overall TCI, as in the case of the pre-cooling system. Figure 9 illustrates the TCI composition for the minimum LCOH solutions. In this scenario, the GREEN-EMS requires a total investment of 10.32 M€, while the MIXED-EMS achieves a lower investment of 6.64 M€ (35.66% reduction).

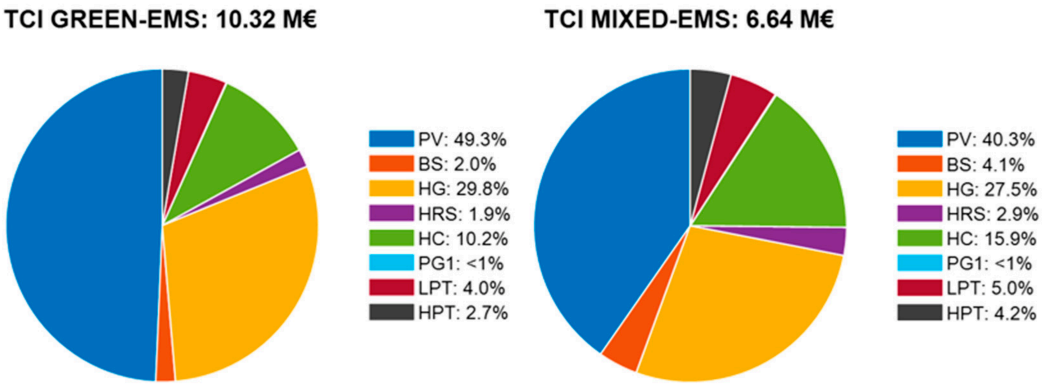

Figure 9. Breakdown of the total capital investment for the lowest LCOH configurations.

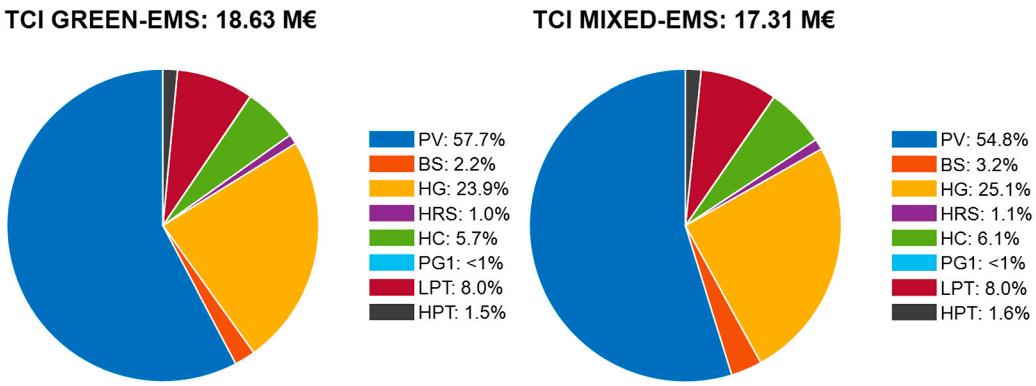

Figure 10. Breakdown of the total capital investment for the highest SSR configurations.

The PV system represents the dominant cost component, accounting for 49.3% (GREEN-EMS) and 40.3% (MIXED-EMS) of the total investment. The HG contributes significantly, with 29.8% and 27.5% respectively, while the contribution of the BS remains limited to 2% and 4.1%. The lower total cost of the MIXED-EMS is primarily attributed to the smaller PV installation required. Although the PV system represents similar percentages in both cases, its absolute investment is significantly lower in the MIXED-EMS because of the smaller installed capacity. The possibility of relying on grid electricity also eliminates the need for oversized renewable generation.

Figure 10 shows the TCI breakdown for the configurations with an SSR of 100%. In this case, the investment requirements increase substantially: the GREEN-EMS reaches 18.63 M€ (80.5% increase relative to the minimum LCOH configuration), whereas the MIXED-EMS reaches 17.31 M€ (160.69% increase). The most notable change is the increased dominance of the PV system, which now represents 57.7% and 54.8% of the TCI, respectively. This shift reflects the need for significantly oversized photovoltaic capacity to ensure energy autonomy even during periods of low solar irradiation. The contribution of the BS also increases slightly to 2.2% and 3.2%, while the HG contribution decreases in relative terms (23.9% and 25.1%) despite maintaining similar absolute values. The larger percentage increase in the MIXED-EMS investment (160.69% vs. 80.5%) indicates that achieving self-sufficiency is particularly challenging and costly when starting from a grid-dependent optimum, as the system requires a more substantial redesign of its energy sources.

3.3. Parametric Analysis by Varying the HG Cost Coefficient

A further cost analysis was conducted by varying the HG cost coefficient, which is expected to decrease in the coming years [40,41]. As reported in Table 4, the baseline value of c_{HG} considered so far is 3165.72 € $kW^{-0.885}$. Three additional coefficient values were therefore considered, while the cost correlation was kept unchanged: 1191.48 € $kW^{-0.885}$, the value forecast for 2030 according to [40]; 545.69 € $kW^{-0.885}$, the value forecast for 2050 with a total installed capacity of 1 TW [41]; and 353.54 € $kW^{-0.885}$, the value also forecast for 2050 but with a total installed power of 5 TW [41].

A multi-objective optimization was therefore performed by varying the HG cost coefficient for the GREEN- and MIXED-EMS, with the same settings used for the previous optimization. The results are shown in Figure 11. The blue curve refers to the first optimization and to the baseline coefficient considered (also shown in Figure 4 for GREEN-EMS and in Figure 8 for MIXED-EMS), while the other curves relate to the new costs considered. As expected, decreasing the HG cost coefficient reduces the LCOH.

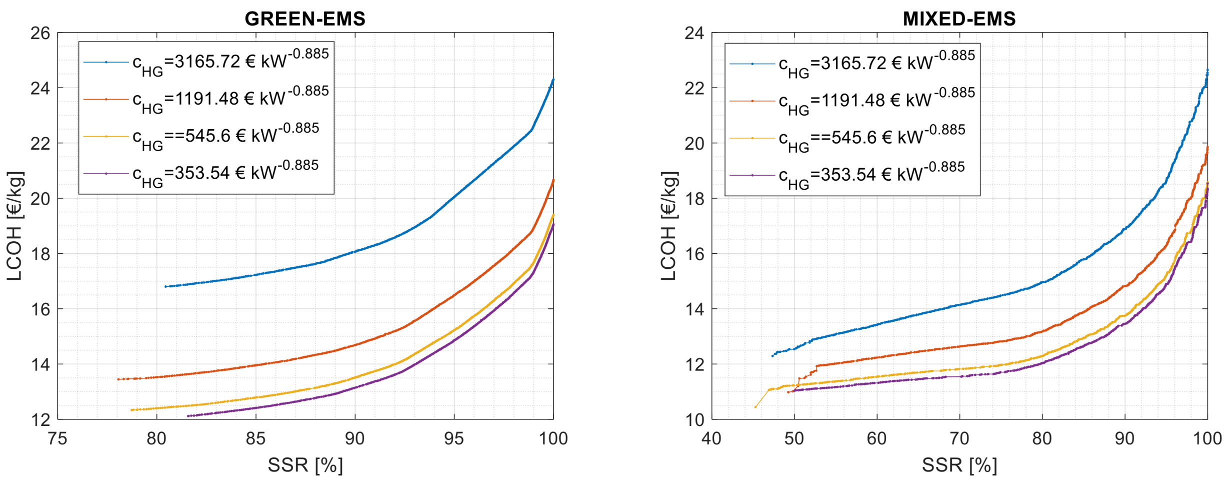

Figure 11. Optimization results by varying the HG cost coefficient.

Table 6 reports the main results for GREEN-EMS, including the component sizes, for each HG cost coefficient considered. Considering an SSR of 100%, the cost decreases from 24.3 €/kg to a minimum of 19.06 €/kg (without selling the surplus electricity). In general terms, the values found for the component sizes are similar to each other: the PV has a size ranging between 8353 kW and 8421 kW, the BS has a size ranging between 312 kWh and 403 kWh, the HG has a size ranging between 2909 kW and 2981 kW, and the LPT has a size ranging between 435.9 m^3 and 462.2 m^3. For the maximum-SSR solutions, it is expected that the variation in HG cost coefficient has no impact, as this parameter does not influence the SSR objective function. However, when analyzing the opposite extreme (LCOH minimization scenarios), a clear trend emerges as the HG cost coefficient decreases from 3165.72 € $kW^{-0.885}$ to 353.54 € $kW^{-0.885}$: the electrolyzer size increases from 1917 kW to 2429 kW (+26.7%), while the PV installation decreases from 3978 kW to 3568 kW (minimum value). This indicates that, when the minimization of LCOH is the objective, lower electrolyzer costs make it economically favorable to shift the system design toward a larger hydrogen generation capacity and reduced photovoltaic oversizing, as the optimizer balances the capital costs between the two main components.

Table 6. Optimization results and component sizes by varying the HG cost: GREEN-EMS.

	Case	c_{HG}	SSR	LCOH	LCOH′ (0.1 €/kWh)	LCOH′ (0.15 €/kWh)	PV	BS	HG	LPT
		[€ kW$^{-0.885}$]	[%]	[€/kg]	[€/kg]	[€/kg]	[kW]	[kWh]	[kW]	[m^3]
1	Min LCOH	3165.72	80.44	16.8	15.63	15.04	3978	198	1917	128
2	Max SSR		100	24.3	17.98	14.92	8398	384	2909	462
3	Min LCOH	1191.48	78.06	13.45	12.84	12.55	3545	191	2151	131
4	Max SSR		100	20.66	14.5	11.42	8421	312	2950	460
5	Min LCOH	545.69	78.73	12.33	11.74	11.45	3568	172	2332	144
6	Max SSR		100	19.4	13.33	10.3	8369	403	2981	436
7	Min LCOH	353.54	81.58	12.12	11.27	10.85	3849	184	2429	140
8	Max SSR		100	19.06	13	9.97	8353	360	2974	457

In this case, the reduction in the LCOH was analyzed by considering the sale of surplus electricity produced, limiting the analysis to a selling price of 0.10 €/kWh (close to the regional weighted average) and 0.15 €/kWh (close to the national average). Considering the higher selling price (0.15 €/kWh), the results show a reduction of 9.24 €/kg by 2030 and approximately 9.1 €/kg by 2050 in both scenarios.

Table 7 reports the main results for MIXED-EMS, including the component sizes, for each HG cost coefficient considered. Considering an SSR of 100%, the cost decreases from 22.68 €/kg to a minimum of 17.41 €/kg, without selling the surplus electricity. As for the GREEN-EMS, the component sizes remain similar as the HG cost coefficient changes: the PV has a size ranging between 7153 kW and 7408 kW, the BS has a size ranging between 389.4 kWh and 530 kWh, the HG has a size ranging between 2758 kW and 2967 kW, and the LPT has a size ranging between 412.3 m^3 and 451 m^3. Analyzing the opposite extreme (LCOH minimization scenarios), the electrolyzer size increases from 1051 kW to 1688 kW (+60.6%), while the PV installation decreases from 2279 kW to 1996 kW (minimum value). Also in this case, the reduction in the LCOH was analyzed by considering the sale of surplus electricity produced, limiting the analysis to selling prices of 0.10 €/kWh (close to the regional weighted average) and 0.15 €/kWh (close to the national average). Considering the highest selling price (0.15 €/kWh), the results show a reduction between 6.88 €/kg (2050, both scenarios) and 6.97 €/kg (2030).

Table 7. Optimization results and component sizes by varying the HG cost: MIXED-EMS.

	Case		SSR	LCOH	LCOH′ (0.1 €/kWh)	LCOH′ (0.15 €/kWh)	PV	BS	HG	LPT
		[€ kW$^{-0.885}$]	[%]	[€/kg]	[€/kg]	[€/kg]	[kW]	[kWh]	[kW]	[m^3]
1	Min LCOH	3165.72	47.34	12.29	11.97	11.81	2088	258	1064	103
2	Max SSR		100	22.68	17.93	15.56	7408	530	2835	431
3	Min LCOH	1191.48	49.25	10.16	9.11	8.59	2279	181	1051	70
4	Max SSR		100	19.05	14.40	12.08	7338	450	2878	451
5	Min LCOH	545.69	45.28	9.63	8.71	8.25	2032	152	1688	71
6	Max SSR		100	17.77	13.18	10.89	7301	412	2967	446
7	Min LCOH	353.54	45.28	9.41	8.49	8.03	1996	141	1593	69
8	Max SSR		100	17.41	12.83	10.53	7153	389	2758	412

3.4. Comparison with the Results Obtained for the GRID-EMS

The performance obtained for the two proposed EMSs are finally compared with the performance achieved when hydrogen was produced exclusively using electricity purchased from the grid. The compared values refer to the baseline HG cost coefficient, and the LCOH was evaluated without considering revenues from electricity exports. Since no green hydrogen is produced in this case, the sole minimization of the LCOH is considered during the optimization process. The LCOH found in this case is 12.13 €/kg, with an HG of 1605 kW and an LPT of 106.5 m^3 (PV and BS are not present). A summary of the results found for each EMS is reported in Table 8.

Table 8. Comparison of the results obtained for the GREEN-, MIXED- and GRID-EMS.

	Case	EMS	SSR [%]	LCOH [€/kg]	PV [kW]	BS [kWh]	HG [kW]	LPT [m^3]	CO_2 [kt/year]
1	Min LCOH	GREEN-EMS	80.44	16.8	3978	198	1917	128.1	0.016
2	LCOH=LCOH (Case 7)		99.04	22.68	7420	300.5	2886	445.4	0.021
3	Max SSR		100	24.3	8398	384	2909	462.2	0.019
4	Min LCOH	MIXED-EMS	47.34	12.29	2088	258.4	1064	102.7	0.710
5	SSR=SSR (Case1)		80.44	14.98	3778	248	1889	218.4	0.292
6	LCOH=LCOH (Case1)		89.66	16.81	4858	328.3	2101	254.9	0.179
7	Max SSR		100	22.68	7408	529.7	2834	430.7	0.037
8	Min LCOH	GRID-EMS	-	12.13	-	-	1605	106.5	1.323

In particular, the results obtained for the two objective functions are reported together with the sizing of the main microgrid components and SSR. The table also reports the annual CO_2 emissions for the different cases, obtained by multiplying the annual amount of electricity purchased from the public grid by the average emission factor for Italian electricity production in 2025, equal to 0.22 kg CO_2/kWh [42]. Considering the results obtained for the configurations with an SSR equal to 100%, comparing the results obtained with a GREEN-EMS (Case 3) and with a MIXED-EMS (Case 7), the values found for the LCOH and for the components are similar, with a slightly lower LCOH value found for the case of MIXED-EMS (22.68 €/kg vs. 24.3 €/kg) due to the smaller sizes of the PV, HG and LPT.

Looking at the results obtained for the lowest LCOH (Case 1 adopting GREEN-EMS, Case 4 adopting MIXED-EMS), the lowest value is again obtained for the MIXED-EMS (12.29 €/kg vs. 16.8 €/kg). However, the SSR for the MIXED-EMS is, in this case, lower than that found for the GREEN-EMS: in fact, while, with the GREEN-EMS, the SSR is about 80.44% (but the remaining 19.56% is not satisfied), for the MIXED-EMS, the value decreases up to 47.34%, while the remaining HRS demand is satisfied with hydrogen produced by using the public grid (52.66%). Regarding the component sizes for the MIXED-EMS, all component sizes except the BS capacity are smaller, especially the PV size: this means that the lower cost of purchasing a smaller PV, HG and LPT system outweighs the cost of energy purchased from the grid.

Two additional MIXED-EMS configurations were analyzed: Case 6 characterized by an LCOH close to the lowest value found for the GREEN-EMS, and Case 5 characterized by the same SSR as the minimum-LCOH GREEN-EMS configuration. For the first case, the SSR is higher than the value found for the GREEN-EMS (89.66% vs. 80.44%) due to the larger component sizes. At the same SSR, the MIXED-EMS achieves a lower LCOH than the GREEN-EMS (14.98 €/kg versus 16.8 €/kg) because of the smaller PV and HG capacities.

Finally, starting from the MIXED-EMS point with the greater LCOH of 22.68 €/kg, the point of the GREEN-EMS with the same cost was analyzed (Case 2): an SSR of 99.04% was therefore found. Considering this SSR acceptable for the HRS, the two configurations are approximately equivalent in terms of both LCOH and SSR. However, since the GREEN-EMS is characterized by significantly lower CO_2 emissions, this solution is preferable. As expected, the lowest LCOH is obtained by producing hydrogen directly from electricity purchased from the grid (Case 8), i.e., 12.13 €/kg. In this case, the hydrogen generator is not limited by the capacity factor of the PV system, and it can operate continuously, resulting in a downsizing of this component due to its greater utilization factor and a substantial reduction in the hydrogen storage capacity required. However, as expected, this case is also characterized by higher emissions: 1.323 kt CO_2/year. Compared to the previously reported emissions of diesel buses, 1.50 kt CO_2/year, this means that replacing 21 diesel buses with hydrogen ones leads to a reduction of approximately 12%. The emissions reduction increases to 52.6% for the minimum-LCOH MIXED-EMS configuration and to 97.5% for the maximum-SSR MIXED-EMS configuration. For the maximum-SSR GREEN-EMS configuration, annual emissions decrease to approximately 0.019 kt CO_2/year, corresponding to a reduction of 98.7%. It should be noted that the residual emissions in the GREEN-EMS are attributable to the use of grid electricity to meet the HRS auxiliary electricity demand when renewable generation is insufficient.

To provide a clearer overview of the optimized system operation, the annual electricity and hydrogen balances corresponding to the representative configurations reported in Table 8 are summarized in Table 9.

Table 9. Annual energy flows obtained for the GREEN-, MIXED- and GRID-EMS.

	Case	EMS	E_{PV} [MWh]	E_{FG} [MWh]	E_{TG} [MWh]	E_{HG} [MWh]	$m_{HRS,del}$ [t]
1	Min LCOH	GREEN-EMS	5728	73.4	1217	4445	80.6
2	LCOH=LCOH (Case 7)		10,685	96.1	4816	5748	98.5
3	Max SSR		12,093	86.2	6138	5821	100.2
4	Min LCOH	MIXED-EMS	3007	3225	323	5777	100.2
5	SSR=SSR (Case1)		5440	1325	701	5870	100.2
6	LCOH=LCOH (Case1)		6996	815	1739	5867	100.2
7	Max SSR		10,668	167	4760	5850	100.2
8	Min LCOH	GRID-EMS	0	6013	0	5836	100.2

Each row of Table 9 refers to the same optimized configuration presented in the corresponding row of Table 8. The table reports the annual PV electricity production (E_{PV}), the electricity purchased from the public grid (E_{FG}), the surplus electricity exported to the grid (E_{TG}), the electricity consumed by the hydrogen generator (E_{HG}), and the annual amount of hydrogen delivered by the HRS ($m_{HRS,del}$). As expected, the annual energy balance reflects the different operating strategies adopted by the three EMSs. In the GREEN-EMS, electricity purchased from the grid is limited to supplying the HRS auxiliary loads, while hydrogen production is entirely based on renewable electricity. Consequently, increasing the SSR from 80.44% to 100% requires progressively larger PV systems, leading to a significant increase in both PV electricity generation and surplus electricity exported to the grid. In the MIXED-EMS, part of the hydrogen demand is satisfied using electricity purchased from the public grid, resulting in lower PV generation and lower surplus electricity exports for the configurations with lower SSR. Unlike the GREEN-EMS analysis, where the hydrogen demand is not always completely satisfied, the integration with the public grid guarantees that the HRS hydrogen demand is fully met in all representative MIXED-EMS configurations, with an annual hydrogen production of approximately 100 t/year in every scenario. As the target SSR increases, the contribution of renewable electricity progressively replaces grid electricity, and the annual energy flows approach those obtained for the GREEN-EMS. Finally, in the GRID-EMS, hydrogen production relies exclusively on electricity purchased from the public grid, with no PV generation or electricity exported to the grid.

A particular note must be made on the costs obtained. These, in fact, are higher than those commonly found in the literature: [43] reports an LCOH close to 8 €/kg for hydrogen production using PV and grid electricity with a PEM HG, while [44] reports an LCOH between 3.5 €/kg and 10.4 €/kg for hydrogen production from PV. However, some important aspects of the case study analyzed should be underlined: the renewable-based microgrid is exclusively used for the HRS, and thus, the PV electrical generation is limited by the current HG demand. Furthermore, the cost is strongly influenced by the hydrogen production rate, which amounts to approximately 100 t/year. Therefore, to further investigate the influence of the hydrogen production scale on the LCOH, two additional optimizations were performed for the GREEN-EMS considering only the minimization of the LCOH. Starting from the baseline case, in which the HRS refueling period was assumed to be 6 h/day, the daily hydrogen demand was doubled and tripled by extending the refueling period to 12 and 18 h/day, respectively, while maintaining the same hourly hydrogen demand. The main results are summarized in Table 10. Increasing the annual hydrogen demand reduces the minimum LCOH from 16.80 €/kg in the baseline case to 15.16 €/kg for the doubled demand and 14.90 €/kg for the tripled demand. These results indicate a clear diminishing marginal benefit of increasing the HRS utilization rate. However, the reduction in LCOH is accompanied by a substantial decrease in renewable self-sufficiency. When the optimization is driven exclusively by LCOH minimization, the increase in hydrogen demand therefore favors higher system utilization and a lower specific hydrogen cost but at the expense of the share of demand that can be supplied using renewable electricity.

Table 10. Sensitivity of GREEN-EMS configuration to the annual hydrogen demand.

HRS Refueling Period [h/day]	H_2 Demand [t/year]	SSR [%]	LCOH [€/kg]	PV [kW]	BS [kWh]	HG [kW]	LPT [m^3]
6	100.25	80.4	16.8	3978	198	1917	128.1
12	200.5	49.4	15.16	5951	100	3000	129
18	300.75	29.2	14.9	5991	123	3000	50

A final analysis of the results concerns the comparison between the LCOH obtained by producing hydrogen exclusively from the public grid (12.13 €/kg, Table 8) and the corrected LCOH′ calculated considering the sale of surplus renewable electricity at the highest price (0.15 €/kWh in Table 6). The results suggest that, under the cost scenarios expected for 2030 and 2050, hydrogen production based solely on renewable sources could become economically more advantageous than production based on grid electricity. Specifically, in 2030, the production cost is lower (11.42 €/kg versus 12.13 €/kg from the grid), while in 2050, it decreases further to 10.3 €/kg or 9.97 €/kg. This reduction is mainly attributable to the projected decrease in the HG cost and to the additional revenue derived from selling surplus renewable electricity. However, it should be emphasized that this projected cost reduction is based on the current national average electricity price for the first quarter of 2025. Therefore, the actual extent of the cost decrease will also depend on the future evolution of electricity market prices.

4. Conclusions

This paper investigated the integration of an optimized HRS into a renewable energy-based microgrid. A mathematical model was developed in MATLAB to evaluate the microgrid performance under different Energy Management Strategies (EMSs), each characterized by an increasing share of green hydrogen production. Three EMSs were investigated: the GREEN-EMS, characterized by hydrogen production exclusively from renewable sources; the MIXED-EMS, which combines renewable and grid-based production; and the GRID-EMS, with hydrogen produced solely using grid electricity. Each EMS was optimized to determine the optimal component sizing with respect to two objective functions: maximizing the SSR and minimizing the LCOH. Initial results showed that, at an SSR of 100%, the GREEN-EMS exhibited a higher LCOH of 24.3 €/kg compared with 22.68 €/kg for the MIXED-EMS. These costs were significantly reduced when accounting for surplus electricity sales to the grid: at the highest electricity selling price (0.15 €/kWh), the LCOH decreased to 14.92 €/kg (GREEN-EMS) and 15.56 €/kg (MIXED-EMS). For the GREEN- and MIXED-EMS, a parametric analysis was conducted by varying the HG cost coefficient, with projections for 2030 and 2050. Results showed a cost reduction to 9.97 €/kg (GREEN-EMS) and to 10.53 €/kg (MIXED-EMS) by 2050, assuming current electricity selling prices remain stable at the higher selling price (0.15 €/kWh).

The PV system was the dominant component of the TCI, accounting for 49.3% and 40.3% in the minimum LCOH configurations of the GREEN- and MIXED-EMS, respectively. These contributions increased to 57.7% and 54.8% at an SSR of 100%, as the total investments increased by 80.5% for the GREEN-EMS and 160.69% for the MIXED-EMS because of the oversized renewable capacity required to achieve full self-sufficiency. The GRID-EMS resulted in an LCOH of approximately 12.13 €/kg. This indicates that, by 2050, renewable-based hydrogen production could become more cost-competitive than grid-based production, provided that the projected HG cost reductions are achieved and electricity selling prices remain relatively stable. Under the current cost assumptions, however, an additional cost of approximately 2.8 €/kg must be considered for renewable hydrogen production compared with grid-based production, even when the highest electricity selling price is considered.

Regarding CO_2 emissions, the current fleet of 21 diesel buses is responsible for about 1.50 kt CO_2 /year. The GRID-EMS results in annual emissions of approximately 1.32 kt CO_2/year, corresponding to an 11.7% reduction. The emissions decrease substantially as the renewable contribution increases, with reductions of up to 97.5% for the MIXED-EMS and 98.7% for the GREEN-EMS. It is worth noting that these quantitative results are specific to the investigated case study and depend on the assumed hydrogen-demand profile, electricity purchase and selling prices, surplus electricity revenues, and future equipment-cost projections. Variations in these assumptions may lead to higher or lower LCOH values, particularly for the 2030 and 2050 scenarios. Therefore, the reported values should be interpreted as scenario-dependent estimates rather than universally applicable results, although the general trends and conclusions of this study remain valid.

Author Contributions: Conceptualization, R.T., M.P. and M.M.; methodology, R.T. and M.P.; software, R.T.; validation, M.P. and M.M.; formal analysis, R.T. and M.P.; investigation, R.T.; writing—original draft preparation, R.T.; writing—review and editing, M.P. and M.M.; visualization, R.T. and M.P.; supervision, M.P.; funding acquisition, M.M. All authors have read and agreed to the published version of the manuscript.

Funding: The authors acknowledge support from the University of Cagliari under Open Access funding call for the publication of this work.

Data Availability Statement: The raw data supporting the conclusions of this article will be made available by the authors on request.

Conflicts of Interest: The authors declare no conflict of interest.

Abbreviations

The following abbreviations are used in this manuscript:

Symbols

AA	Active Area
c	Cost parameter
E	Energy [Wh]
f	Derating Factor [-]
GI	Global Irradiance [W/m^2]
HHV	Higher Heating Value [J/kg]

IR	Interest Rate [%]
LOH	Level Of Hydrogen [-]
m	Mass [kg]
$\dot{m}$	Mass flow rate [kg/s]
OM	Operating and Maintenance cost rate
P	Electric Power [W]
SOC	State Of Charge [-]
t	Time [h]
T	Temperature [°C]
TCI	Total Capital Investment [€]
U	Heat transfer coefficient [W/m^2/K]
y	Project lifetime [year]
α	Absorptance coefficient [-]
γ	Temperature coefficient [-]
η	Efficiency [-]
τ	Transmittance coefficient [-]
Subscripts	
A	Ambient conditions
C	Cell
EC	Engineering Cost
FG	From Grid
H_2	Hydrogen
INV	Inverter
MOD	PV Module
$NOCT$	Nominal Operating Cell Temp.
NOM	Nominal conditions
STC	Standard Test Conditions
TG	To Grid
Acronyms	
BEV	Battery Electric Vehicle
BOP	Balance Of Plant
BS	Battery Storage
DOD	Depth Of Discharge
EMS	Energy Management Strategy
FCEV	Fuel Cell Electric Vehicle
GHG	Greenhouse Gases
GHI	Global Horizontal Irradiance
HC	Hydrogen Compressor
HG	Hydrogen Generator
HRS	Hydrogen Refueling Station
HT	Hydrogen Tank
HPT	High-Pressure Tank
ICE	Internal Combustion Engine
LCOE	Levelized Cost Of Electricity
LCOH	Levelized Cost Of Hydrogen
LPT	Low-Pressure Tank
PC	Pre-Cooling
PEC	Purchase Equipment Cost
PEM	Proton Exchange Membrane
PG	Public Grid
PV	Photovoltaic
SSR	Self-Sufficiency Rate
VT	Vehicle Tank
WT	Wind Turbine

References

1. Csalódi, R.; Czvetkó, T.; Sebestyén, V.; Abonyi, J. Sectoral Analysis of Energy Transition Paths and Greenhouse Gas Emissions. *Energies* **2022**, *15*, 7920. [CrossRef]
2. Crippa, M.; Guizzardi, D.; Pagani, F.; Banja, M.; Muntean, M.; Schaaf, E.; Becker, W.; Monforti-Ferrario, F.; Quadrelli, R.; Risquez Martin, A. *GHG Emissions of All World Countries*; Publications Office of the European Union: Luxembourg, 2024; p. 273. [CrossRef]
3. Global Fuel Economy Initiative. Trends in The Global Vehicle Fleet 2023—Managing The SUV Shift and The EV Transition. 2023. Available online: https://www.globalfueleconomy.org/media/na1pjian/gfei-trends-in-the-global-vehicle-fleet-2023-spreads.pdf (accessed on 22 August 2025).
4. Gürbüz, H. Analysis of the operating characteristics of hydrogen PEM fuel cell and battery on electric vehicle in different driving cycles. *Environ. Prog. Sustain. Energy* **2023**, *42*, e14146. [CrossRef]
5. Pergamalis, C.; Tsampasis, E.; Dedes, I.C.; Elias, C. Hydrogen Fuel Cell Electrical Vehicles (FCEV)—Battery Electric Vehicles (BEV)—Comparison and Future Challenges. In Proceedings of the 2024 13th Mediterranean Conference on Embedded Computing, MECO 2024, Budva, Montenegro, 11–14 June 2024. [CrossRef]
6. Aguilar, P.A.; Groß, B. Battery Electric Vehicles and Fuel Cell Electric Vehicles, an Analysis of Alternative Powertrains as a Mean to Decarbonise the Transport Sector. *SSRN Electron. J.* **2022**, *53*, 102624. [CrossRef]
7. International Energy Agency. Global Hydrogen Review 2024. Available online: https://iea.blob.core.windows.net/assets/89c1e3-82-dc59-46ca-aa47-9f7d41531ab5/GlobalHydrogenReview2024.pdf (accessed on 21 July 2025).
8. International Energy Agency. Global Electric Vehicles Outlook 2025. Available online: https://iea.blob.core.windows.net/assets/-7ea38b60-3033-42a6-9589-71134f4229f4/GlobalEVOutlook2025.pdf (accessed on 21 July 2025).
9. Hossain Bhuiyan, M.M.; Siddique, Z. Hydrogen as an alternative fuel: A comprehensive review of challenges and opportunities in production, storage, and transportation. *Int. J. Hydrogen Energy* **2025**, *102*, 1026–1044. [CrossRef]
10. Grazieschi, G.; Zubaryeva, A.; Sparber, W. Energy and greenhouse gases life cycle assessment of electric and hydrogen buses: A real-world case study in Bolzano Italy. *Energy Rep.* **2023**, *9*, 6295–6310. [CrossRef]
11. Fragiacomo, P.; Genovese, M.; Piraino, F.; Massari, F.; Boroomandnia, M. Analysis of a distributed green hydrogen infrastructure designed to support the sustainable mobility of a heavy-duty fleet. *Int. J. Hydrogen Energy* **2024**, *51*, 576–594. [CrossRef]
12. Okonkwo, P.C.; Mansir, I.B.; Barhoumi, E.M.; Emori, W.; Radwan, A.B.; Shakoor, R.A.; Uzoma, P.C.; Pugalenthi, M.R. Utilization of renewable hybrid energy for refueling station in Al-Kharj, Saudi Arabia. *Int. J. Hydrogen Energy* **2022**, *47*, 22273–22284. [CrossRef]
13. Parsibenehkohal, R.; Jamil, M.; Khan, A.A. A multi-stage framework for coordinated scheduling of networked microgrids in active distribution systems with hydrogen refueling and charging stations. *Int. J. Hydrogen Energy* **2024**, *71*, 1442–1455. [CrossRef]
14. Ancona, M.A.; Catena, F.; Ferrari, F. Optimal design and management for hydrogen and renewables based hybrid storage microgrids. *Int. J. Hydrogen Energy* **2023**, *48*, 20844–20860. [CrossRef]
15. Şafak, B.; Çiçek, A. Multi-Objective Optimal Energy Management Strategy for Grid-Interactive Hydrogen Refueling Stations in Rural Areas. *Sustainability* **2025**, *17*, 2663. [CrossRef]
16. Sun, W.; Harrison, G.P. Active Load Management of Hydrogen Refuelling Stations for Increasing the Grid Integration of Renewable Generation. *IEEE Access* **2021**, *9*, 101681–101694. [CrossRef]
17. Al-Sharafi, A.; Al-Buraiki, A.S.; Al-Sulaiman, F.; Antar, M.A. Hydrogen refueling stations powered by hybrid PV/wind renewable energy systems: Techno-socio-economic assessment. *Energy Convers. Manag. X* **2024**, *22*, 100584. [CrossRef]
18. Rizk-Allah, R.M.; Hassan, I.A.; Snasel, V.; Hassanien, A.E. An optimal standalone wind-photovoltaic power plant system for green hydrogen generation: Case study for hydrogen refueling station. *Results Eng.* **2024**, *22*, 102234. [CrossRef]
19. Di Micco, S.; Minutillo, M.; Perna, A.; Jannelli, E. On-site solar powered refueling stations for green hydrogen production and distribution: Performances and costs. *E3S Web Conf.* **2022**, *334*, 01005. [CrossRef]
20. Barhoumi, E.M.; Okonkwo, P.C.; Ben Belgacem, I.; Zghaibeh, M.; Tlili, I. Optimal sizing of photovoltaic systems based green hydrogen refueling stations case study Oman. *Int. J. Hydrogen Energy* **2022**, *47*, 31964–31973. [CrossRef]
21. Bahou, S. Techno-economic assessment of a hydrogen refuelling station powered by an on-grid photovoltaic solar system: A case study in Morocco. *Int. J. Hydrogen Energy* **2023**, *48*, 23363–23372. [CrossRef]
22. Hussain, S.; Daneshmand, S.V.; Zareipour, H.; Layzell, D.; Khan, A. Optimal Sizing of a Stand-alone Renewable-Powered Hydrogen Fueling Station. In Proceedings of the 2022 IEEE International Autumn Meeting on Power, Electronics and Computing, ROPEC 2022, Ixtapa, Mexico, 9–11 November 2022. [CrossRef]
23. Kavadias, K.A.; Kosmas, V.; Tzelepis, S. Sizing, Optimization, and Financial Analysis of a Green Hydrogen Refueling Station in Remote Regions. *Energies* **2022**, *15*, 547. [CrossRef]
24. Gu, Y.; Chen, Q.; Xue, J.; Tang, Z.; Sun, Y.; Wu, Q. Comparative techno-economic study of solar energy integrated hydrogen supply pathways for hydrogen refueling stations in China. *Energy Convers. Manag.* **2020**, *223*, 113240. [CrossRef]
25. Tang, O.; Rehme, J.; Cerin, P. Levelized cost of hydrogen for refueling stations with solar PV and wind in Sweden: On-grid or off-grid? *Energy* **2022**, *241*, 122906. [CrossRef]

26. Yaowang, P.; Fengxiang, C. Real-time water content regulation in PEMFC shutdown via MPC with SH-AUKF-based state feedback: Towards improved efficiency and reduced energy consumption. *eTransportation* **2025**, *25*, 100461. [CrossRef]
27. Tatti, R.; Petrollese, M.; Cau, G. Techno-economic analysis and optimization of a hydrogen refueling station integrated in a renewable-based microgrid. In Proceedings of the 37th International Conference on Efficiency, Cost, Optimization, Simulation and Environmental Impact of Energy Systems, Rhodes, Greece, 30 June–5 July 2024. [CrossRef]
28. Safra Group. HYCITY®: Hydrogen Bus—Safra. Available online: https://safra.fr/en/hycity-en/ (accessed on 3 September 2025).
29. Meteonorm. Available online: https://meteonorm.com/en/ (accessed on 15 October 2025).
30. Cells, Q. Q-PEAK DUO-G9 335–355 W. Available online: https://www.vpsolar.com/download/catalog/Moduli/QCells/Q.PEAK-DUO-G9/Q_CELLS_Specifiche_Q.PEAK_DUO-G9_QD_335-355_2021-01_Rev01_IT.pdf (accessed on 12 October 2025).
31. Duffie, J.A.; Beckman, W.A. *Solar Engineering of Thermal Processes: Fourth Edition*; John Wiley & Sons: Hoboken, NJ, USA, 2013. [CrossRef]
32. Serra, F.; Lucariello, M.; Petrollese, M.; Cau, G. Optimal Integration of Hydrogen-Based Energy Storage Systems in Photovoltaic Microgrids: A Techno-Economic Assessment. *Energies* **2020**, *13*, 4149. [CrossRef]
33. Saferna, A.; Saferna, P.; Kuczyński, S.; Łaciak, M.; Szurlej, A.; Włodek, T. Effects of Hydrogen, Methane, and Their Blends on Rapid-Filling Process of High-Pressure Composite Tank. *Energies* **2024**, *17*, 1130. [CrossRef]
34. Micena, R.P.; Llerena-Pizarro, O.R.; de Souza, T.M.; Silveira, J.L. Solar-powered Hydrogen Refueling Stations: A techno-economic analysis. *Int. J. Hydrogen Energy* **2020**, *45*, 2308–2318. [CrossRef]
35. Elgowainy, A.; Reddi, K.; Lee, D.Y.; Rustagi, N.; Gupta, E. Techno-economic and thermodynamic analysis of pre-cooling systems at gaseous hydrogen refueling stations. *Int. J. Hydrogen Energy* **2017**, *42*, 29067–29079. [CrossRef]
36. Khan, M.A.; Young, C.; MacKinnon, C.; Layzell, D. *The Techno-Economics of Hydrogen Compression*; Transition Accelerator Technical Briefs; The Transition Accelerator: Calgary, AB, Canada, 2021; Volume 1, Issue 1, pp. 1–36.
37. MathWorks. MATLAB Gamultiobj—Find Pareto front of Multiple Fitness Functions Using Genetic Algorithm. Available online: https://uk.mathworks.com/help/gads/gamultiobj.html (accessed on 30 October 2025).
38. GSE. Pagamenti Ritiro Dedicato: Calcolo, Fatture E Dichiarazioni Fiscali. Available online: https://www.gse.it/servizi-per-te/fotovoltaico/ritiro-dedicato/regolazione-economica-del-servizio#consultare (accessed on 10 October 2025).
39. GSE. Prezzi Medi Mensili Per Fascia Oraria E Zona Di Mercato. 2025. Available online: https://www.gse.it/documenti_site/Documenti%20GSE/Servizi%20per%20te/RITIRO%20DEDICATO/Altri%20contenuti/Prezzi%20medi%20RID%202025.pdf (accessed on 9 October 2025).
40. Reksten, A.H.; Thomassen, M.S.; Møller-Holst, S.; Sundseth, K. Projecting the future cost of PEM and alkaline water electrolysers; a CAPEX model including electrolyser plant size and technology development. *Int. J. Hydrogen Energy* **2022**, *47*, 38106–38113. [CrossRef]
41. IRENA (International Renewable Energy Agency). *Green Hydrogen Cost Reduction: Scaling up Electrolysers to Meet the 1.5 °C Climate Goal*; IRENA (International Renewable Energy Agency): Abu Dhabi, United Arab Emirates, 2020; p. 105. Available online: https://www.irena.org/publications/2020/Dec/Green-hydrogen-cost-reduction (accessed on 9 October 2025).
42. ISPRA. *Settore Elettrico: Emissioni Di* CO_2 *e Altri Impatti. Edizione 2026*; ISPRA: Rome, Italy, 2026. Available online: https://www.isprambiente.gov.it/files2026/pubblicazioni/rapporti/r430-2026-2.pdf (accessed on 30 July 2026).
43. Bhandari, R.; Shah, R.R. Hydrogen as energy carrier: Techno-economic assessment of decentralized hydrogen production in Germany. *Renew. Energy* **2021**, *177*, 915–931. [CrossRef]
44. Frieden, F.; Leker, J. Future costs of hydrogen: A quantitative review. *Sustain. Energy Fuels* **2024**, *8*, 1806–1822. [CrossRef]